Cell Stress and Chaperones (2022) 27:461–478
https://doi.org/10.1007/s12192-022-01279-9

ORIGINAL ARTICLE

Extracellular Hsp90α stimulates a unique innate gene profile in microglial cells with simultaneous activation of Nrf2 and protection from oxidative stress

Yuka Okusha[1,2] · Benjamin J. Lang[1] · Ayesha Murshid[1] · Thiago J. Borges[3] · Kristina M. Holton[4,5] · Joanne Clark-Matott[6] · Sachin Doshi[1] · Tsuneya Ikezu[7] · Stuart K. Calderwood[1]

Received: 1 March 2022 / Revised: 1 May 2022 / Accepted: 15 May 2022 / Published online: 10 June 2022

Abstract

Delivery of exogenous heat shock protein 90α (Hsp90α) and/or its induced expression in neural tissues has been suggested as a potential strategy to combat neurodegenerative disease. However, within a neurodegenerative context, a pro-inflammatory response to extracellular Hsp90α (eHsp90α) could undermine strategies to use it for therapeutic intervention. The aim of this study was to investigate the biological effects of eHsp90α on microglial cells, the primary mediators of inflammatory responses in the brain. Transcriptomic profiling by RNA-seq of primary microglia and the cultured EOC2 microglial cell line treated with eHsp90α showed the chaperone to stimulate activation of innate immune responses in microglia that were characterized by an increase in NF-kB-regulated genes. Further characterization showed this response to be substantially lower in amplitude than the effects of other inflammatory stimuli such as fibrillar amyloid-β (fAβ) or lipopolysaccharide (LPS). Additionally, the toxicity of conditioned media obtained from microglia treated with fAβ was attenuated by addition of eHsp90α. Using a co-culture system of microglia and hippocampal neuronal cell line HT22 cells separated by a chamber insert, the neurotoxicity of medium conditioned by microglia treated with fAβ was reduced when eHsp90α was also added. Mechanistically, eHsp90α was shown to activate Nrf2, a response which attenuated fAβ-induced nitric oxide production. The data thus suggested that eHsp90α protects against fAβ-induced oxidative stress. We also report eHsp90α to induce expression of macrophage receptor with collagenous structure (Marco), which would permit receptor-mediated endocytosis of fAβ.

Keywords Hsp90 · Extracellular HSPs · Nrf2 · NF-kB · Inflammation · Microglia · Amyloid-beta · Marco

Introduction

Heat shock proteins (HSPs) promote protein homeostasis (proteostasis) via fulfilling several protein quality-control functions (Lang 2021). Collectively, the actions of HSPs and

Yuka Okusha, Benjamin J. Lang and Ayesha Murshid contributed equally to this work

✉ Yuka Okusha
yokusha@bidmc.harvard.edu

✉ Stuart K. Calderwood
scalderw@bidmc.harvard.edu

[1] Department of Radiation Oncology, Beth Israel Deaconess Medical Center, Harvard Medical School, Boston, MA 02215, USA

[2] JSPS Overseas Research Fellowship, Tokyo 102-0083, Japan

[3] Center for Transplantation Sciences, Department of Surgery, Massachusetts General Hospital, Harvard Medical School, Boston, MA 02129, USA

[4] Research Computing, Harvard Medical School, Boston, MA 02215, USA

[5] Department of Stem Cell and Regenerative Biology, Harvard University, Cambridge, MA 02138, USA

[6] Department of Neurology, Beth Israel Deaconess Medical Center, Harvard Medical School, Boston, MA 02215, USA

[7] Department of Neuroscience, Molecular NeuroTherapeutics Laboratory, Mayo Clinic Florida, Jacksonville, FL 32224, USA

other molecular chaperones prevent the formation of protein aggregates and solubilize existing aggregates. Failure of these functions has particular significance in the emergence of neurodegenerative diseases caused by the build-up of amyloid deposits. Overexpression of various HSPs has been shown to protect against protein aggregation in vivo (Rampelt et al. 2012; Fujimoto et al. 2005). The observed decline of HSP expression in neural tissue with aging has further indicated their importance in maintaining proteostasis (Garigan et al. 2002; Hsu et al. 2003). This finding has indicated a potential opportunity for therapeutic intervention through increased local concentrations of HSPs as an approach to combatting protein aggregation in neurodegenerative disease. One such strategy utilizes heat shock response (HSR)–inducing compounds to increase tissue HSP levels, an approach that may be constrained by the relatively weak capacity for neurons to activate heat shock factor 1 (HSF1), the key transcription factor for stress-induced HSP expression (Calderwood and Murshid 2017). However, low levels of HSR activation within neurons may be augmented by uptake of extracellular HSPs (eHSPs) released by surrounding microglia and astrocytes (Guzhova et al. 2001; Tidwell et al. 2004). These findings have led to the concept that the HSR may not be totally cell-intrinsic and that an effective transcellular response may be involved (Taylor et al. 2007). Importantly for neurodegenerative disease, studies have shown HSPs to readily cross the blood–brain barrier and suggest that HSPs may be delivered exogenously and enter the brain space (Kirkegaard et al. 2016). Additionally, induction of HSP expression in other parts of the body may enable increased HSP concentrations within the brain (Oosten-Hawle and Morimoto 2014; Theriault et al. 2006). Canonically, delivery of HSPs increases cellular chaperone levels and also may influence cell phenotype on encountering receptors in target cells (Theriault et al. 2006). In mononuclear phagocytes, the cells under study here, HSPs have been shown to bind to the scavenger receptors. Indeed, a potential risk of HSP therapeutics for neurodegenerative disease is the possibility of inflammation (Zhang et al. 2018; Thawkar and Kaur 2019). Neuroinflammation is a key pathological factor in the etiology of Alzheimer's disease. This response is largely mediated by microglial cells, the resident mononuclear phagocytes of the brain, as they attempt to detoxify beta-amyloid fibrils and necrotic cell bodies and adopt a toxic inflammatory phenotype (Clayton et al. 2017; Krasemann et al. 2017; Yamamoto et al. 2008).

The stress-inducible Hsp90α (encoded by *HSP90AA1*) can be detected in the extracellular space and has also been shown to be protective against protein aggregate formation and disease (Calderwood et al. 2016; Li et al. 2012). Hsp90α binds to the scavenger receptors, but it is not known whether it induces an inflammatory profile in microglial cells. This question has important implications for therapies seeking to increase concentrations of neuronal Hsp90. Our previous studies that examined the role of Hsp90 in immune and inflammatory responses as part of a program to employ the chaperones in cancer immune–based therapies found that although Hsp90 is internalized by target cells such as macrophages and dendritic cells and can facilitate immunity by transporting extracellular antigens into antigen processing cells, its effects were generally not inflammatory (DNA 2006; Hancock et al. 2015; Murshid et al. 2015). Indeed, when we compared the effects on macrophages of LPS with the inflammatory profile of eHsp90α to that of LPS, we found that although eHsp90α triggered many of the same changes in the macrophages as LPS, inflammatory gene expression was minimal. The inflammatory effects of eHsp90 were judged to be stalled by a homeostatic mechanism.

In the present study, we have examined the effects of eHsp90α on gene expression in microglia as part of a program to assess the role of Hsp90 in mediating a potential intercellular HSR in cells of the central nervous system (CNS). Our findings were that eHsp90, although modifying the expression of immune-related genes, also induced several immune-suppressive genes such as the scavenger receptor *Marco* and the immunometabolism regulator *Acod1*. Our data also pointed to the induction by Hsp90 of the transcription factor nuclear factor, erythroid-derived 2, like 2 (Nrf2), which is a central effector of the oxidative stress response and in addition to promoting cell survival, also exerts anti-inflammatory effects.

Materials and methods

Cell culture

The murine microglia cell line BV2, a line of immortalized mouse microglia (Stansley et al. 2012). BV2 cells were maintained in Dulbecco's modified Eagle's medium (DMEM, Gibco, Carlsbad, CA, USA) supplemented by 10% fetal bovine serum (FBS, Gibco, Carlsbad, CA, USA) and penicillin–streptomycin (1000 units/ml, Invitrogen, Carlsbad, CA, USA), non-essential amino acids (Invitrogen, Carlsbad, CA, USA), HEPES (Corning, NY, USA), and monocyte colony–stimulating factor (M-CSF, 20 ng/ml, R&D Systems, Minnesota, MN, USA). The murine microglia cell line EOC2 (CRL-2467) was obtained from American Type Culture Collection (ATCC, Gaithersburg, MD, USA). EOC2 cultures were maintained in DMEM media supplemented with 10% HI FBS, 20% LADMAC conditioned media (ATCC, CRL-2420). Hippocampal neuronal cell line HT22 cells were sourced from ATCC and maintained in DMEM supplemented with 10% FBS, penicillin–streptomycin (1000 units/ml), 2 ml L-glutamine,

and HEPES. Primary murine microglia were cultured and maintained according to Timmerman et al. (2018). Neonatal murine microglia were isolated from P0 CD-1 pups using CD11b microbeads (Ca #130–093-634, Miltenyi Biotec), and their purity was assessed by immunocytochemistry of myeloid cell markers (Iba-1 and CD11b), according to the published method (Ikezu 2020). All the cell cultures were maintained in a 5% CO_2 humidified incubator at 37 °C.

Chemicals and reagents

Recombinant full-length human Hsp90α was expressed by baculovirus in Sf9 insect cells using a C-terminal His tag vector and purified by metal affinity chromatography, as previously described (Murshid et al. 2010). Hsp90 was therefore produced from a source free of endotoxin contamination. His-tag removal was performed using AcTEV protease and passing the proteolytically cleaved Hsp90 through a Ni–NTA purification system (Qiagen, Valencia, CA). The native Hsp90 is collected in the column eluate and used for generation of experimental data shown in Figs. 1, 2, 3A,D, 4, 5A-C,F and 6A; Suppl. Fig. 1; and Suppl. Fig. 2A. For all the other data, the experiments were performed using purchased human C-terminal His-tagged Hsp90α produced in baculovirus Sf9 insect cells (H36-50H, Signalchem, Richmond, BC, USA) and diluted in cell media to 10 µg/ml, and equimolar concentrations of His-tagged protein buffer (NP20-153–01, Signalchem, Richmond, BC) were added to control samples. Mouse Aβ1-42 and Aβ1-40, FITC tagged mouse Aβ1-42, and control peptides were purchased from American Peptides and AnaSpec. Lipopolysaccharide (LPS) was purchased from Sigma-Aldrich, St. Louis, MO, USA. The *Nrf2* inhibitor, ML385 (Medchem Express, Monmouth Junction, NJ, USA) was used to inhibit the *Nrf2* expression in BV2 cells. For experiments using ML385, BV2 cells were seeded (1×10^5 cells) and cultured in 35-mm dishes. The next day, 5 µM ML385 ($ED^{50} = 1.9$ µM) was added in the medium. On the 2nd day of post-ML385 addition, the cells were used for Hsp90α treatment assays.

RNA-seq analysis

RNA-seq analysis was performed following a previously described workflow (Lang et al. 2018). EOC2 cells were treated with or without 10 µg/ml eHsp90α for 4 h at which time RNA was isolated using RNeasy kit (Qiagen). Primary microglia were treated with or without 10 µg/ml eHsp90α for 12 h, and RNA was isolated using the same method. RNA integrity was assessed by using a bioanalyzer (Agilent) with samples with RIN > 7 used for cDNA library synthesis. cDNA library synthesis was performed on ribosome RNA–depleted total RNA using a KAPA stranded RNA-seq with RiboErase (cat. no. KK8483) and Illumina adapters. cDNA libraries were pooled and sequenced with an Illumina HiSeq 2500 (50 cycles, paired-end) to give 10–20 million reads per sample. RNA integrity analysis, cDNA pooling, and NGS services were provided by Harvard Biopolymers Facility. Raw RNA-seq data was processed in a high-performance compute environment using Trimmomatic 0.36 to remove adapters and filter for high-quality reads (Bolger et al. 2014). Read quality was confirmed using FastQC 0.11.5 (Andrews n.d.), and aligned to the *Mus musculus* annotated genome GRCm38 (Frankish et al. 2019), using STAR 2.5.4a aligner with the –quantMode GeneCounts option (Dobin et al. 2013). Using R version > 3.6.2, feature counts were then filtered for features with at least 3 counts per million (cpm) across 4 (EOC2) or 3 (primary microglia) samples, which gave 10,790 and 12,866 remaining features, respectively. Feature counts were then TMM-normalized and differentially expressed genes (DEG) identified and fold changes quantified using the edgeR statistical package (Robinson et al. 2010). Gene ontology analysis was applied to the DEG list using the clusterProfiler package (Yu et al. 2012), which included representations of the enrichGO function for over-representation analysis and gseKEGG and gseGO functions for gene set enrichment analyses. TFEA analysis was performed using the ChEA3 API available at https://maayanlab.cloud/chea3/, where the DEG list (FDR < 0.05) was used as an input for ChEA3 TFEA analysis of the primary microglia dataset and a filtered DEG list (FDR < 0.05, ± logFC > 0.6) was used as input for the EOC2 ChEA3 TFEA analysis (Keenan et al. 2019). The same respective inputs were used for TFEA analysis by HOMER 4.11.1 (Heinz et al. 2010). The HOMER default settings were used with –cpg and –bg options, with the background gene lists specified to genes that had > 3 cpm across 4 (EOC2) or 3 (primary microglia) samples.

Western blot analysis

Western blotting was performed, as previously described (Gong et al. 2018). Briefly, cells were lysed in a RIPA buffer (Boston BioProducts, MA, USA) using 25-gauge syringes. The same protein amounts were subjected to 4–20% gradient gel (Genscript, NJ, USA), followed by transfer to a polyvinylidene fluoride (PVDF) membrane using wet methods where appropriate. The membranes were blocked in a blocking solution (LI-COR, Inc., Lincoln, NE, USA) for 60 min unless otherwise specified, and incubated overnight with a rabbit monoclonal anti-pNrf2 antibody (1/5000, ab76026, Abcam, Cambridge, MA), a mouse monoclonal anti-Nrf2 antibody (1/1000, MAB3925, Biotechne, Minnesota, MN, USA), a rabbit polyclonal anti-Nrf2 antibody (1/1000, NBP1-32,822, Biotechne, Minnesota, MN, USA), a rabbit polyclonal

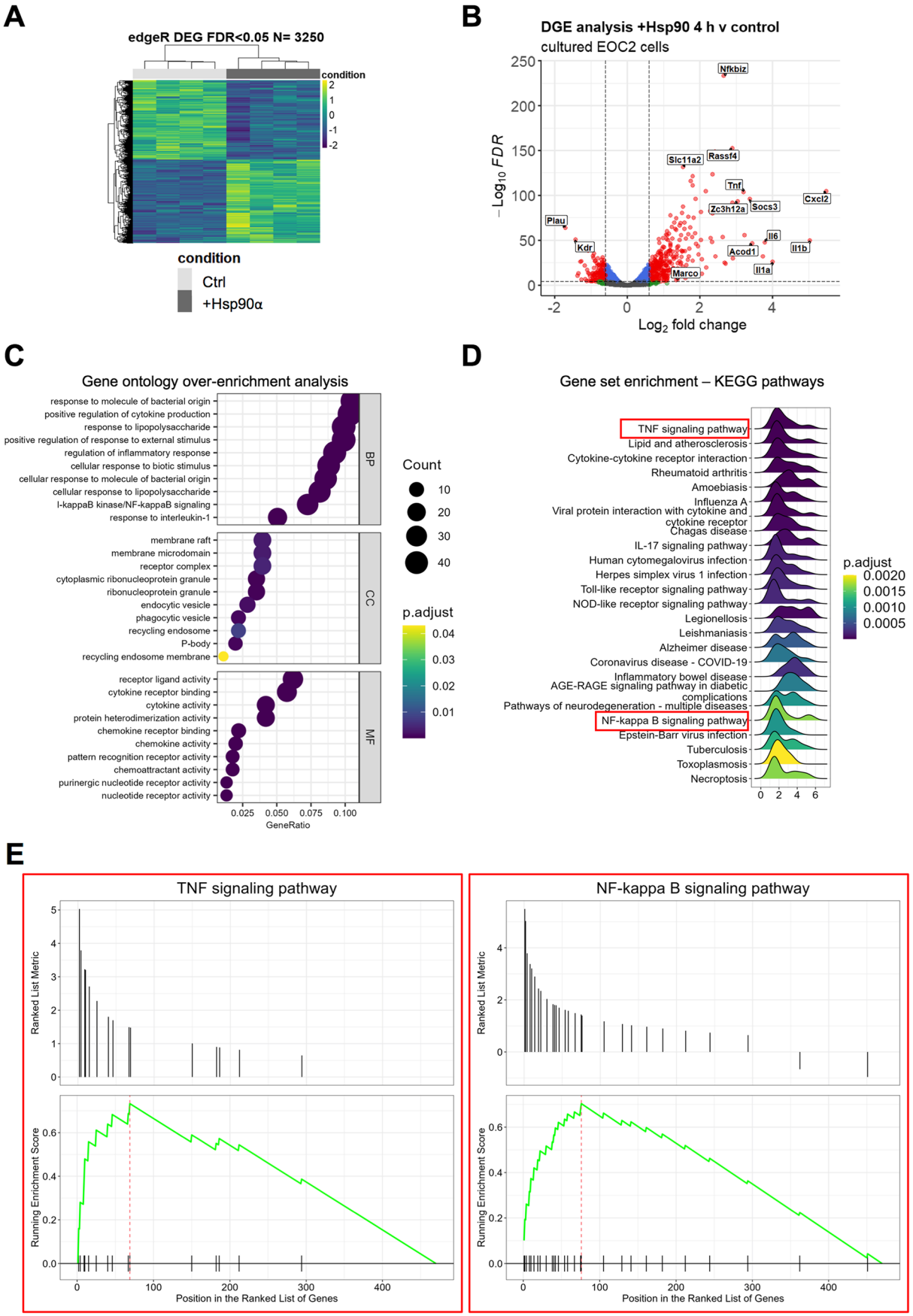
A
edgeR DEG FDR<0.05 N= 3250
condition
2
1
0
-1
-2
condition
Ctrl
+Hsp90α
B
DGE analysis +Hsp90 4 h v control
cultured EOC2 cells
−Log10 FDR
Log2 fold change
Nfkbiz
Slc11a2
Rassf4
Tnf
Cxcl2
Zc3h12a
Socs3
Plau
Kdr
Il6
Il1b
Acod1
Il1a
Marco
C
Gene ontology over-enrichment analysis
response to molecule of bacterial origin
positive regulation of cytokine production
response to lipopolysaccharide
positive regulation of response to external stimulus
regulation of inflammatory response
cellular response to biotic stimulus
cellular response to molecule of bacterial origin
cellular response to lipopolysaccharide
I-kappaB kinase/NF-kappaB signaling
response to interleukin-1
BP
membrane raft
membrane microdomain
receptor complex
cytoplasmic ribonucleoprotein granule
ribonucleoprotein granule
endocytic vesicle
phagocytic vesicle
recycling endosome
P-body
recycling endosome membrane
CC
receptor ligand activity
cytokine receptor binding
cytokine activity
protein heterodimerization activity
chemokine receptor binding
chemokine activity
pattern recognition receptor activity
chemoattractant activity
purinergic nucleotide receptor activity
nucleotide receptor activity
MF
0.025 0.050 0.075 0.100
GeneRatio
Count
10
20
30
40
p.adjust
0.04
0.03
0.02
0.01
D
Gene set enrichment – KEGG pathways
TNF signaling pathway
Lipid and atherosclerosis
Cytokine-cytokine receptor interaction
Rheumatoid arthritis
Amoebiasis
Influenza A
Viral protein interaction with cytokine and cytokine receptor
Chagas disease
IL-17 signaling pathway
Human cytomegalovirus infection
Herpes simplex virus 1 infection
Toll-like receptor signaling pathway
NOD-like receptor signaling pathway
Legionellosis
Leishmaniasis
Alzheimer disease
Coronavirus disease - COVID-19
Inflammatory bowel disease
AGE-RAGE signaling pathway in diabetic complications
Pathways of neurodegeneration - multiple diseases
NF-kappa B signaling pathway
Epstein-Barr virus infection
Tuberculosis
Toxoplasmosis
Necroptosis
0 2 4 6
p.adjust
0.0020
0.0015
0.0010
0.0005
E
TNF signaling pathway
NF-kappa B signaling pathway
Ranked List Metric
Running Enrichment Score
Position in the Ranked List of Genes

Fig. 1

F

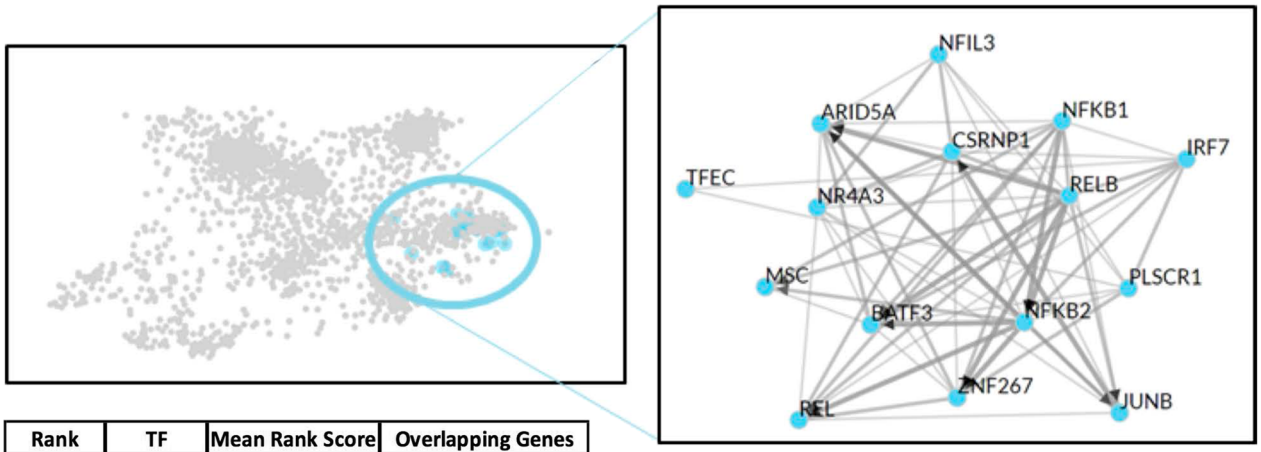

Rank	TF	Mean Rank Score	Overlapping Genes
1	CSRNP1	3.5	69
2	NFKB2	7.25	156
3	RELB	9.25	153
4	BATF3	10	100
5	NR4A3	10	116
6	ZNF267	12.67	121
7	PLSCR1	14	71
8	ARID5A	14.5	60
9	NFKB1	15.75	143
10	MSC	18.67	116
11	NFIL3	24.67	96
12	IRF7	25.67	106
13	TFEC	26.67	93
14	JUNB	26.75	117
15	REL	27	106

G

Rank	Motif	P-value	log P-pvalue	% of Targets	% of Background	STD(Bg STD)	Best Match/Details
1		1e-18	-4.311e+01	12.20%	2.58%	92.5bp (125.0bp)	RELA/MA0107.1/Jaspar(0.940)
2		1e-12	-2.914e+01	2.66%	0.05%	84.2bp (98.6bp)	SMAD3/MA0795.1/Jaspar(0.693)
3		1e-11	-2.680e+01	2.88%	0.10%	101.3bp (107.1bp)	TEAD(TEA)/Fibroblast-PU.1-ChIP-Seq(Unpublished)/Homer(0.702)
4		1e-11	-2.669e+01	6.43%	1.14%	109.2bp (120.0bp)	PB0126.1_Gata5_2/Jaspar(0.607)
5		1e-11	-2.637e+01	2.44%	0.05%	93.2bp (58.4bp)	POL009.1_DCE_S_II/Jaspar(0.656)

Fig. 1 (continued) The transcriptional response to eHsp90α at 4 h is characterized by activation of NF-kB-regulated processes. **A** Heatmap representation of the 3250 DEG (FDR < 0.05) identified by RNA-seq analysis between EOC2 cells treated with 10 µg/ml Hsp90α for 4 h versus untreated control samples. **B** Volcanoplot representing the FDR and logFC values of changes in gene expression between EOC2 cells treated with 10 µg/ml Hsp90α for 4 h versus untreated control samples. Values for features that returned at least 3 counts per million (cpm) across 4 of the 8 samples with MGI symbols are shown. **C** Gene ontology over enrichment analysis was applied to the filtered EOC2 DEG list (FDR < 0.05, ± logFC 0.6) using the enrichGO function of the clusterProfiler package to return enriched descriptive terms belonging to the GO categories; biological process (BP), cellular component (CC), and molecular function (MF). **D** Ridgeplot of gene set enrichment of KEGG pathways performed on the same filtered EOC2 DEG list (FDR < 0.05, ± logFC 0.6) using the clusterProfiler function gseKEGG. Values for the directional expression distribution (x-axis) and Benjamini–Hochberg adjusted *p*-value (p.adjust) are represented. **E** GSEA plots of selected KEGG pathways representing the enrichment scores for the respective gene sets and the positions of genes within the gene set in the ranked DEG list ordered by descending logFC. **F** Results of ChEA3 TFEA analysis showing the top 15 transcription factors in the Global GTEx TF Network (left), the local network (right), and the top 15 TFs ranked by mean rank score (lower). The filtered EOC2 DEG list (FDR < 0.05, ± logFC 0.6) was used as input. **G** The top 5 TFs returned by HOMER TFEA analysis are shown. The filtered EOC2 DEG list (FDR < 0.05, ± logFC 0.6) was used as input with all features that returned at least 3 counts per million (cpm) across 4 of the 8 samples with MGI symbols as the background gene list

anti-Marco antibody (1/1000, orb6345, Biobyt, Cambridge, MA), a rabbit monoclonal anti-p-NF-κB p65 S536 antibody (1/1000, 3033S, Cell Signaling, Danvers, MA, USA), a rabbit monoclonal anti- NF-κB p65 antibody (1/1000, 8242S, Cell signaling, Danvers, MA, USA), a mouse monoclonal anti-p62 antibody (1/1000, ab56416, abcam), and a mouse monoclonal anti-actin antibody (1/20000, A5441, Sigma-Aldrich, MO, USA). The membranes were incubated for 1 h at room temperature with goat anti-rabbit IRDye 800 CW fluorescent secondary antibodies (1/15000, LI-COR, Inc., Lincoln, NE, USA) and 680 RD fluorescent secondary antibodies (1/15000, LI-COR, Inc., Lincoln, NE, USA). Blots were washed with Tris-buffered saline, 0.1% (w/v) Tween 20 (TBS-T), and visualized with the Odyssey Imaging System (LI-COR, Inc., Lincoln, NE, USA). The quantitative densitometric analysis was performed using Image Studio Lite Ver. 5.2 (LI-COR, Inc., Lincoln, NE, USA).

RT-qPCR analysis

Total RNA preparation and RT-qPCR were carried out, as described previously (Gong et al. 2018). The miRNeasy mini kit (Qiagen, Hilden, Germany) was used with DNase (Qiagen, Hilden, Germany). The total RNA concentration was measured by using a micro spectrometer Nanodrop one (Thermo Fisher, Waltham, MA, USA). cDNA synthesis was carried out by using iScript cDNA Synthesis Kit (Bio-Rad, Richmond, CA. USA). Specific primer pairs (Suppl. Table 3) were designed using Primer-BLAST or selected from PrimerBank, and the sequences were verified for the predicted target using Primer-BLAST to the *Mus musculus* RefSeq database (Wang and Seed 2003). Specificity for a single PCR product was confirmed by melt-curve analysis. Real-time qPCR was performed with Applied Biosystems PowerUp SYBR Green Master mix (Thermo Fisher, Waltham, MA, USA) using a StepOne Plus Instrument or 7500 Real-time PCR System (Applied Biosystems) with the cycling conditions 50 °C 2 min and 95 °C 2 min, (95 °C 3 s, 60 °C 30 s, × 40 cycles). Relative mRNA levels to *Actb* or *Rpl32* mRNA levels were quantified by the ΔΔCt method using the formula–fold change = 2 − ΔΔCt. PCR reactions were carried out in triplicate, and the mean values were calculated with the mean ± S.D. of the biological triplicates presented.

Immunofluorescence

Cells were washed in ice-cold PBS, pH 7.4, fixed with 4% paraformaldehyde at room temperature for 10 min, and then permeabilized with 0.1% Triton X-100 for 5 min. The fixed cells were blocked in 3% normal goat serum solution for 30 min and then incubated overnight at 4 °C with rabbit anti-Marco antibody (1/100, orb6345, Biobyt, Cambridge, UK) in 3% normal goat serum solution. Cells were then incubated with anti- rabbit IgG AlexaFluor488 (Cell Signaling Technology, Danvers, MA, USA) for 1 h at room temperature. Cellular nuclei were stained with 4′, 6-diamidino-2-phenylindole (DAPI; Invitrogen, Carlsbad, CA, USA). HT22 neurites were stained using β-tubulin (ab15568, Abcam, Cambridge, MA), and fluorophore-tagged secondary antibodies were used to fluorescently stain the fixed cells, and nuclei were stained with DAPI. Coverslips were mounted with Prolong Gold medium. Slides were scanned using a Zeiss LSM confocal microscope with Zen software with the respective, appropriate filter sets, as previously described (Murshid et al. 2010; Okusha et al. 2020). Neurite growth in Fig. 5F is measured using ImageJ software. To quantify square micrometer–Marco positive signal/cell, positive signal was defined by the fluorescence intensity of the cells above that of cells stained without the primary antibodies added, which was subtracted as background signal.

Preparation of Aβ fibrils

Aβ1-42 was dissolved in DMSO (stock 500 μM) at room temperature and stored at − 20 °C. To this Aβ aliquot, we added 10 mM of HCl at RT, diluting to a final concentration of 100 μM of fAβ1-42. We mixed by vortex for 15 s, transferred the solution to 37 °C, and incubated for 24 h. The fAβ1-42 solution was then incubated for 24 h at 37 °C.

Quantification of nitric oxide production

Nitric oxide (NO) release from cells was measured (using the manufacturer's protocol) in cells incubated with or without f-AB1-42 and in other control samples using a nitric oxide (total) detection kit, (Enzo Cat. no. ADI-917–020).

Cytokine array

Primary microglia culture was treated with or without eHsp90α (10 μg/ml) or fAβ (2 μM) for 12 h. About 100 μg of supernatant was used for each array. Cytokines released from primary microglia treated with Hsp90α/fAβ were quantified after 12-h treatment using proteome profiler mouse cytokine array kit, panel A (R&B Systems, Cat# ARY006), according to manufacturer's protocol. Data shown are from a 5-min exposure of a film. Image analysis was performed using Western Vision Software, https://wvision.com/.

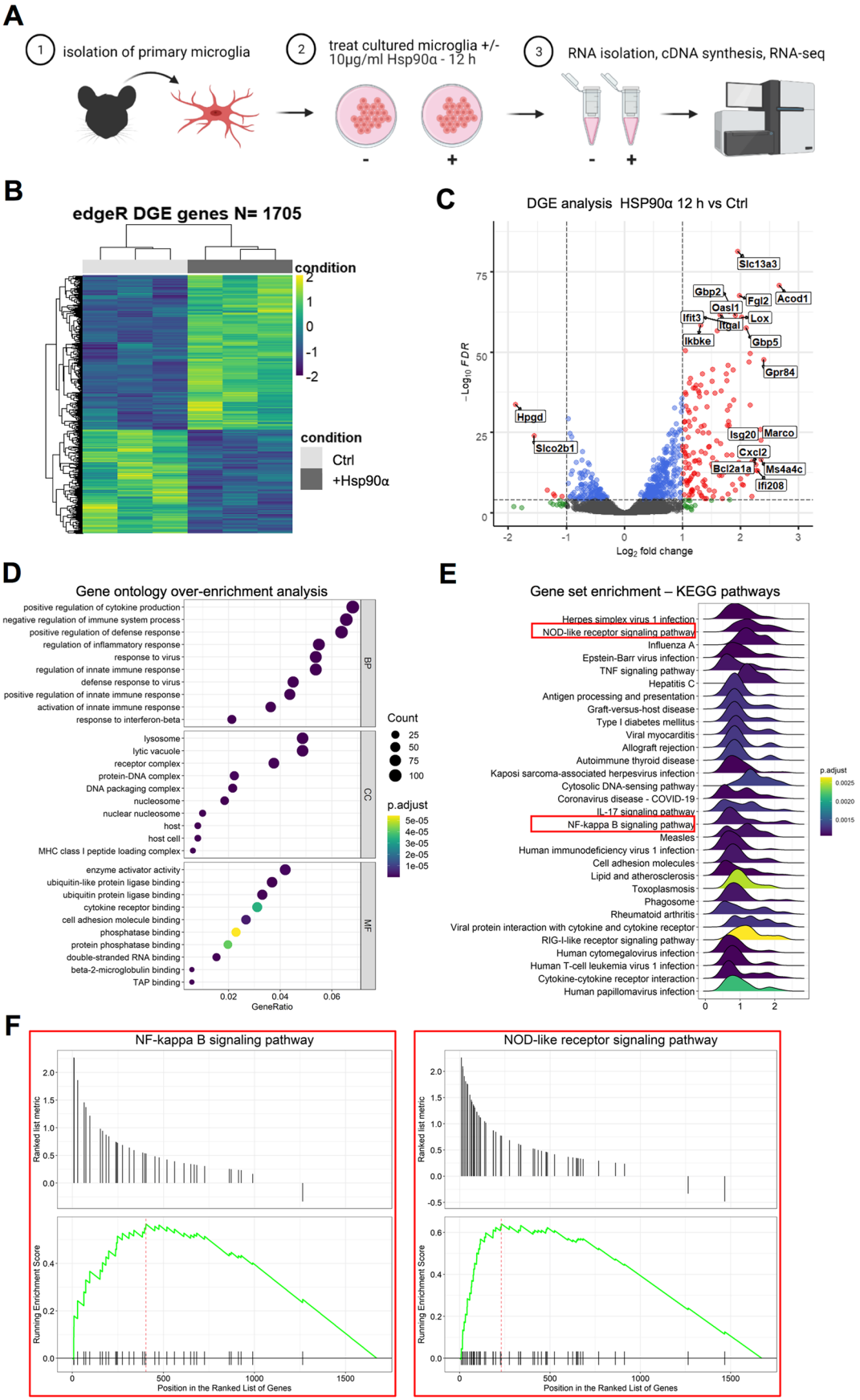
A
1 isolation of primary microglia
2 treat cultured microglia +/- 10µg/ml Hsp90α - 12 h
3 RNA isolation, cDNA synthesis, RNA-seq
- +
- +
B
edgeR DGE genes N= 1705
condition
2
1
0
-1
-2
condition
Ctrl
+Hsp90α
C
DGE analysis HSP90α 12 h vs Ctrl
−Log10 FDR
Log2 fold change
Slc13a3
Gbp2
Fgl2
Acod1
Oasl1
Ifit3
Itgal
Lox
Ikbke
Gbp5
Gpr84
Hpgd
Slco2b1
Isg20
Marco
Cxcl2
Bcl2a1a
Ms4a4c
Ifi208
D
Gene ontology over-enrichment analysis
positive regulation of cytokine production
negative regulation of immune system process
positive regulation of defense response
regulation of inflammatory response
response to virus
regulation of innate immune response
defense response to virus
positive regulation of innate immune response
activation of innate immune response
response to interferon-beta
lysosome
lytic vacuole
receptor complex
protein-DNA complex
DNA packaging complex
nucleosome
nuclear nucleosome
host
host cell
MHC class I peptide loading complex
enzyme activator activity
ubiquitin-like protein ligase binding
ubiquitin protein ligase binding
cytokine receptor binding
cell adhesion molecule binding
phosphatase binding
protein phosphatase binding
double-stranded RNA binding
beta-2-microglobulin binding
TAP binding
BP
CC
MF
Count
25
50
75
100
p.adjust
5e-05
4e-05
3e-05
2e-05
1e-05
GeneRatio
E
Gene set enrichment – KEGG pathways
Herpes simplex virus 1 infection
NOD-like receptor signaling pathway
Influenza A
Epstein-Barr virus infection
TNF signaling pathway
Hepatitis C
Antigen processing and presentation
Graft-versus-host disease
Type I diabetes mellitus
Viral myocarditis
Allograft rejection
Autoimmune thyroid disease
Kaposi sarcoma-associated herpesvirus infection
Cytosolic DNA-sensing pathway
Coronavirus disease - COVID-19
IL-17 signaling pathway
NF-kappa B signaling pathway
Measles
Human immunodeficiency virus 1 infection
Cell adhesion molecules
Lipid and atherosclerosis
Toxoplasmosis
Phagosome
Rheumatoid arthritis
Viral protein interaction with cytokine and cytokine receptor
RIG-I-like receptor signaling pathway
Human cytomegalovirus infection
Human T-cell leukemia virus 1 infection
Cytokine-cytokine receptor interaction
Human papillomavirus infection
p.adjust
0.0025
0.0020
0.0015
F
NF-kappa B signaling pathway
NOD-like receptor signaling pathway
Ranked list metric
Running Enrichment Score
Position in the Ranked List of Genes

Fig. 2

G

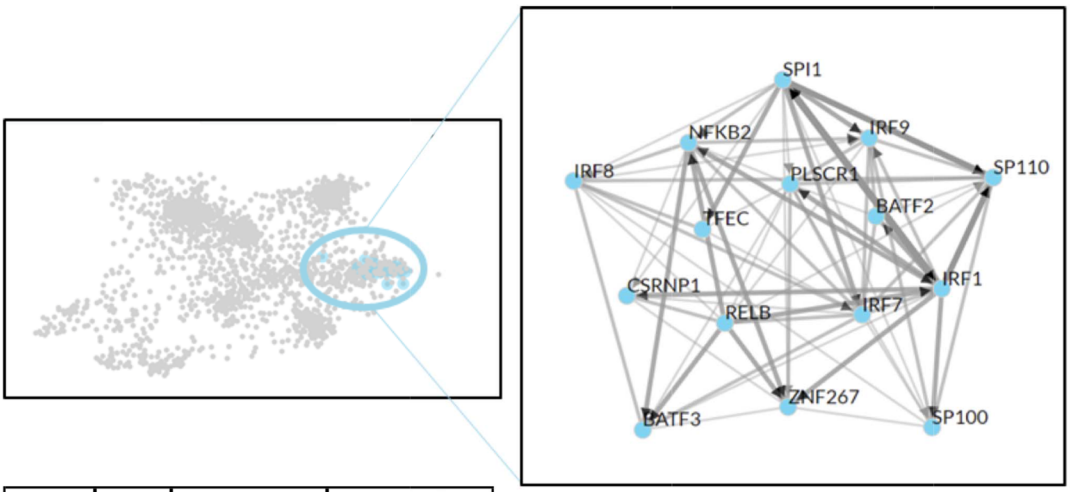

Rank	TF	Mean Rank Score	Overlapping Genes
1	PLSCR1	3.5	197
2	BATF2	8	266
3	IRF7	8.667	262
4	RELB	9	363
5	TFEC	10	253
6	NFKB2	12	348
7	IRF9	12	354
8	IRF1	14.5	628
9	ZNF267	18.67	238
10	CSRNP1	19	143
11	IRF8	19.75	292
12	SPI1	20	535
13	SP110	21.33	222
14	SP100	21.67	227
15	BATF3	22.67	210

H

Rank	Motif	P-value	log P-pvalue	% of Targets	% of Background	STD(Bg STD)	Best Match/Details
1		1e-39	-9.015e+01	7.87%	1.38%	76.9bp (128.2bp)	IRF3(IRF)/BMDM-Irf3-ChIP-Seq(GSE67343)/Homer(0.971)
2		1e-16	-3.733e+01	2.05%	0.16%	101.0bp (87.8bp)	ZNF768(Zf)/Rajj-ZNF768-ChIP-Seq(GSE111879)/Homer(0.641)
3		1e-13	-3.120e+01	8.26%	3.66%	94.1bp (105.0bp)	RELA/MA0107.1/Jaspar(0.939)
4		1e-12	-2.982e+01	3.84%	1.05%	89.3bp (111.5bp)	PB0134.1_Hnf4a_2/Jaspar(0.700)
5		1e-12	-2.852e+01	1.22%	0.05%	87.1bp (104.1bp)	RUNX3/MA0684.2/Jaspar(0.669)

Fig. 2 (continued)

◀ **Fig. 2** eHsp90α stimulates a transcriptional response upon immunological process-related genes in cultured murine primary microglial cells. **A** Schematic describing a simplified workflow employed for isolation and RNA-seq analysis of murine primary microglia treated with or without 10 µg/ml Hsp90α for 12 h. **B** Heatmap representation of the 1705 DEG (FDR < 0.05) identified by RNA-seq analysis between primary microglial cells treated with 10 µg/ml Hsp90α for 12 h versus untreated control samples. **C** Volcanoplot representing the FDR and logFC values of changes in gene expression between primary microglial cells treated with 10 µg/ml Hsp90α for 12 h versus untreated control samples. Values for features that returned at least 3 counts per million (cpm) across 3 of the 6 samples with MGI symbols are shown. **D** Gene ontology over enrichment analysis was applied to the primary microglia DEG list (FDR < 0.05) using the enrichGO function of the clusterProfiler package to return enriched descriptive terms belonging to the GO categories; biological process (BP), cellular component (CC), and molecular function (MF). **E** Ridgeplot of gene set enrichment of KEGG pathways performed on the primary microglia DEG list (FDR < 0.05) using the clusterProfiler function gseKEGG. Values for the directional expression distribution (x-axis) and Benjamini–Hochberg adjusted *p*-value (p.adjust) are represented. **F** GSEA plots of selected KEGG pathways representing the enrichment scores for the respective gene sets and the positions of genes within the gene set in the ranked DEG list ordered by descending logFC. **G** Results of ChEA3 TFEA analysis showing the top 15 transcription factors in the Global GTEx TF Network (left), the local network (right), and the top 15 TFs ranked by mean rank score (lower). The primary microglia DEG list (FDR < 0.05) was used as input. **H** The top 5 TFs returned by HOMER TFEA analysis are shown. The primary microglia DEG list (FDR < 0.05) was used as input with all features that returned at least 3 counts per million (cpm) across 3 of the 6 samples with MGI symbols as the background gene list

Cytokine array image analysis

Array images were collected using an X-ray film and analyzed using image processing software. A template was created to analyze pixel density in each spot of the array. Signal values were exported to a Microsoft Excel spread for plotting. Average signal (pixel density) intensity was measured for two spots where duplicate spots/dots represent one cytokine/chemokine. Averaged background signal was subtracted from each spot. We used a signal from a clear area of the array or negative control spots as a background value. Values are normalized to cytokine levels in the culture media of untreated samples (control).

Statistical analysis

Statistical significance was calculated using JMP Pro 15 and Microsoft Excel. Three or more mean values were compared using one-way analysis of variance (ANOVA), followed by Tukey's post hoc test to determine *p*-values between experimental groups. Statistical significance between two experimental groups was performed using Student's *t*-test. $*p < 0.05$, $**p < 0.01$, $***p < 0.001$, $****p < 0.0001$ was considered to indicate statistical significance. Data were expressed as mean ± SD, unless otherwise specified.

Results

The transcriptional response to eHsp90α is characterized by activation of NF-kB-regulated processes

To examine the immediate transcriptional response to eHsp90α, we performed RNA-seq analysis on murine EOC2 microglial cells cultured with or without eHsp90α for 4 h. Differential expression analysis identified 3250 genes to be significantly altered (FDR < 0.05) in the eHsp90α-treated group versus the non-treated control (Fig. 1A). While examining the most differentially expressed genes by logFC, it was observed that genes most sensitive to eHsp90α treatment tended to be induced (327 genes FDR < 0.05, + logFC 0.6) rather than repressed (164 genes FDR < 0.05, − logFC 0.6), with greatest effect-sizes generally observed in the induced genes (Fig. 1B; Suppl. Table 1). To gain insight into cellular processes most sensitive to eHsp90α, over-enrichment analysis was applied to the differential gene expression (DGE) list filtered for a bidirectional fold-change greater than 1.5 (FDR < 0.05, ± logFC 0.6), which returned a list of 470 differentially expressed genes (DEG) with MGI symbols. This analysis indicated that eHsp90α stimulates altered gene expression of mRNAs involved in various immunological and inflammatory processes (Fig. 1C). Similarly, KEGG pathway enrichment analysis also indicated the altered activity of pathways involved in immunity and inflammation (Fig. 1D), including the TNF and NF-κB signaling pathways (Fig. 1E). To further examine potential effector molecules responsive to eHsp90α, we next applied transcription factor enrichment analysis (TFEA) to the filtered DGE list (FDR < 0.05, ± logFC 0.6) using both ChEA3 (Fig. 1F) and HOMER (Fig. 1G) (Keenan et al. 2019; Heinz et al. 2010). Consistent with the KEGG pathway enrichment analysis, factors of the NF-κB family were identified by both TFEA tools to be among the most significantly altered activity in response to eHsp90α (NFKB2, RELB, NFKB1, REL) (Fig. 1F) and RELA (Fig. 1G). Taken together, the predominant transcriptional response to eHsp90α at 4 h was found to center upon NF-κB regulated processes including altered expression of genes with functional roles in inflammation and immunity.

eHsp90α stimulates a transcriptional response upon immunological process-related genes in primary murine microglial cells

To further characterize the transcriptional response of microglial cells to eHsp90α, we next compared the transcriptomic

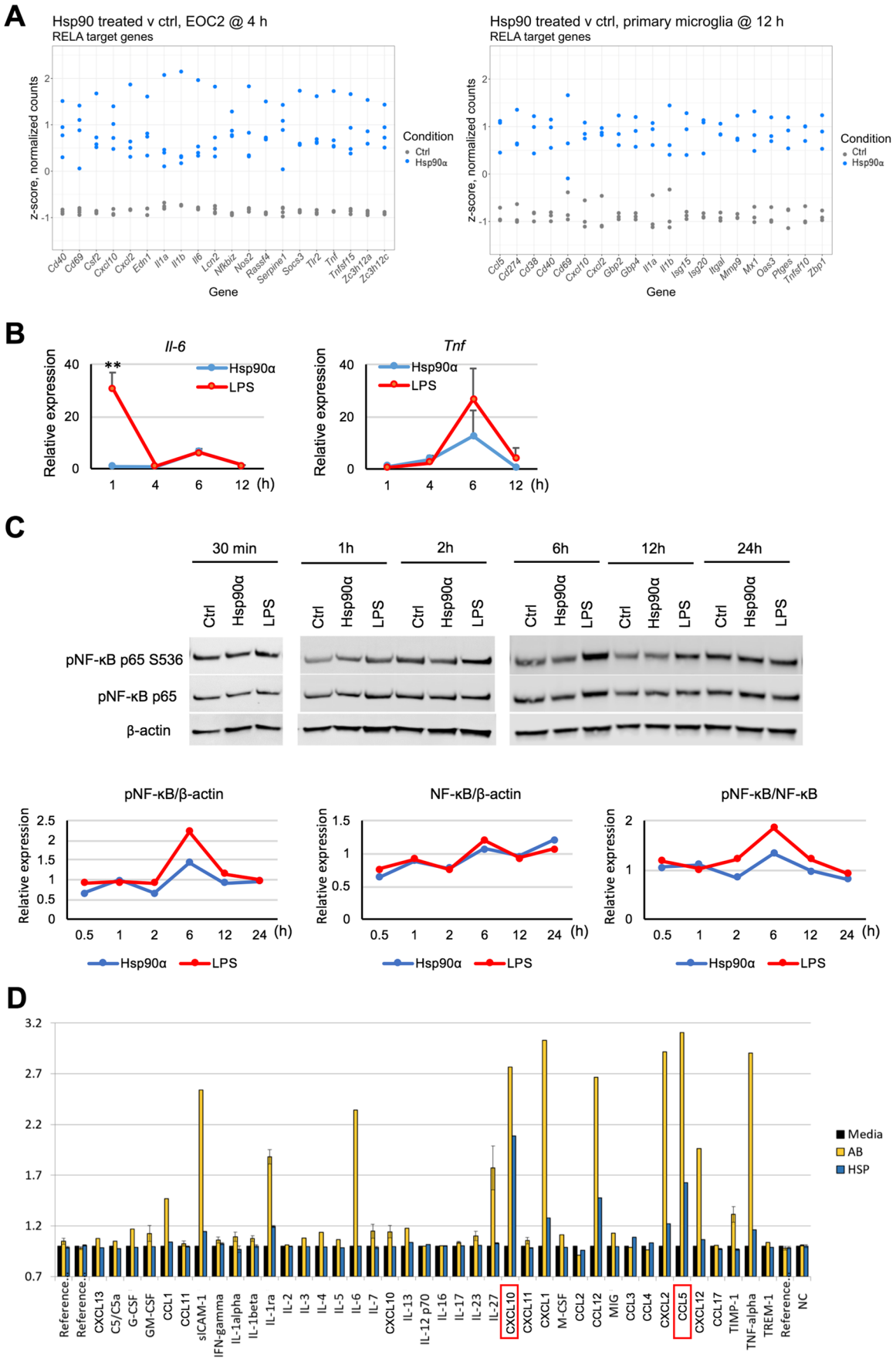
A
Hsp90 treated v ctrl, EOC2 @ 4 h
RELA target genes
z-score, normalized counts
Condition
Ctrl
Hsp90α
Cd40 Cd69 Csf2 Cxcl10 Cxcl2 Edn1 Il1a Il1b Il6 Lcn2 Nfkbiz Nos2 Rassf4 Serpine1 Socs3 Tlr2 Tnf Tnfsf15 Zc3h12a Zc3h12c
Gene
Hsp90 treated v ctrl, primary microglia @ 12 h
RELA target genes
Ccl5 Cd274 Cd38 Cd40 Cd69 Cxcl10 Cxcl2 Gbp2 Gbp4 Il1a Il1b Isg15 Isg20 Itgal Mmp9 Mx1 Oas3 Ptgs Tnfsf10 Zbp1
B
Il-6
Tnf
Relative expression
Hsp90α
LPS
**
1 4 6 12 (h)
C
30 min 1h 2h 6h 12h 24h
Ctrl Hsp90α LPS
pNF-κB p65 S536
pNF-κB p65
β-actin
pNF-κB/β-actin
NF-κB/β-actin
pNF-κB/NF-κB
0.5 1 2 6 12 24 (h)
D
Media
AB
HSP
Reference. Reference. CXCL13 C5/C5a G-CSF GM-CSF CCL1 CCL11 sICAM-1 IFN-gamma IL-1alpha IL-1beta IL-1ra IL-2 IL-3 IL-4 IL-5 IL-6 IL-7 CXCL10 IL-13 IL-12 p70 IL-16 IL-17 IL-23 IL-27 CXCL10 CXCL11 CXCL1 M-CSF CCL2 CCL12 MIG CCL3 CCL4 CXCL2 CCL5 CXCL12 CCL17 TIMP-1 TNF-alpha TREM-1 Reference. NC

◂**Fig. 3** NF-kB target genes are induced in response to eHsp90α, with limited NF-KB activation compared to LPS. **A** Relative levels of mRNAs in EOC2 cells and primary microglia treated with or without 10 µg/ml Hsp90α for 4 h or 12 h, respectively, that were found to be differentially expressed and that have been identified as NF-κB p65 (*RELA*) regulatory targets within the curated datasets of the Chea3 TFEA software. The top 10 genes ranked by absolute logFC are shown. **B** BV2 were cultured in 2% FBS media and treated with Hsp90α (10 µg/ml) or LPS (1000 ng/ml) for 1, 4, 6, and 12 h at which time RNA was isolated and quantified by qPCR for the indicated mRNAs. Gene expression is shown relative to *Actb* and normalized to control untreated RNA samples collected at the same time points. Control samples were treated with an equimolar concentration of His-tagged protein buffer sourced from the same vendor as the His-tagged Hsp90α. **C** Under the same culture and treatment conditions as (**B**), BV2 cells were lysed with RIPA buffer at 30 min, 1, 2, 6, 12, and 24-h post-treatment and cell lysates were analyzed by western blot. Quantitative analyses of immunoblots for p-NF-κB p65 S536, NF-κB p65 are shown with p-NF-κB p65 S536 normalized to total p-NF-κB p65 levels and p-NF-κB p65 levels normalized to β-actin. Each expression ratio was normalized to control untreated samples collected at the same time points. **D** Cytokines released from primary microglia treated with Hsp90α (10 µg/ml) or fAβ (2 µM) were quantified after 12-h treatment using proteome profiler mouse cytokine array kit, according to manufacturer's protocol. Cytokine spots' image intensities are normalized to cytokine levels in culture media of untreated samples (normalized to 1)

profiles of primary microglia treated with or without eHsp90α. We reasoned that the use of primary microglia may provide additional confidence in identification of eHsp90α-responsive genes in microglia when considered with data derived from EOC2 cells, while also allowing for the examination of the response to eHsp90α at a later time-point. The primary microglia were isolated, and the cultures were treated with or without 10 µg/ml eHsp90α for 12 h in triplicate, at which time RNA was isolated and analyzed by RNA-seq analysis (Fig. 2A). Differential gene expression analysis identified 1705 differentially expressed genes (FDR < 0.05) between the eHsp90α-treated and non-treated control conditions (Fig. 2B). Like changes observed in treated EOC2 cells, a cohort of genes exhibited a robust relative increase in mRNA levels in response to eHsp90α (Fig. 2C). Over-representation analysis revealed gene ontology terms again describing processes related to inflammation, infection, and immunity (Fig. 2D), together suggesting some level of innate activation of the eHsp90α-treated microglia. This was also indicated by KEGG pathway analysis, which identified pathways associated with contexts of immune activation (Fig. 2E). The NF-κB signaling pathway was again identified among processes to be altered in response to eHsp90α, in addition to the NOD-like receptor signaling pathway which is mechanistically connected to NF-κB (Fig. 2E, F). Components of the NF-κB transcriptional machinery were also among the top identified factors when TFEA analysis was applied to the DEG list (FDR < 0.05) (Fig. 2G, H). This data indicates that the predominant microglial response to eHsp90α is that of an increase in genes with functions in inflammation and immunity and that NF-κB is a likely driver of this transcriptional response.

NF-kB target genes are induced in response to eHsp90α, with moderate NF-κB activation compared to LPS

As significant research efforts have been directed towards understanding the inflammatory nature of extracellular HSPs (Calderwood et al. 2016), we next sought to further validate and characterize the apparent responsiveness of NF-κB to eHsp90α. We first identified the NF-κB-regulated genes most altered by eHsp90α in the RNA-seq analyses (Fig. 3A) and examined their responsiveness to eHsp90α in cultured murine BV2 microglial cells. RT-qPCR quantitation of NF-κB targets IL-6 *(Il6)* and TNF-α (*Tnf*) was performed on BV2 cultures treated with or without 10µg/ml eHsp90α treatment over a 12-h period (Fig. 3B). These qPCR analyses indicated both *Il6* and *Tnf* mRNA responses to eHsp90α peaked at 6 h, while markedly more robust responses were seen in response to 1000 ng/ml LPS for *Il-6* at 1 h and for *Tnf* at 6 h (Fig. 3B). The NF-κB p65 protein (encoded by *RelA*) forms heterodimers with the proteolytically processed forms of p105/p50 (*Nfkb1*) or p100/p52 (*Nfkb2*). The NF-κB p65/p50 dimer is considered the prototypical form; however, the other REL members RelB (*RelB*) or c-Rel (*Rel*) also form dimers with p50 or p52. To further characterize the relative activation of NF-κB by eHsp90α, we compared the levels of NF-κB p65 activating phosphorylation at serine 536 in BV2 cells treated with eHsp90α to levels of cells treated with LPS (Fig. 3C). NF-κB p65 becomes phosphorylated at Ser536 by the IKK kinases in response to various inflammatory stimuli and is considered indicative of NF-κB activation, reviewed in Huang et al. (2010). A modest increase in pNF-κB levels was detected in response to eHsp90α, the magnitude to which was lower than that stimulated by LPS at 6 h under the experimental conditions used (Fig. 3C). To further examine the possibility that eHsp90α leads to a moderated innate/inflammation response, we also measured the cytokine profile of cultured BV2 cells treated with eHsp90α or the inflammatory stimuli amyloid-beta (Aβ) (Fig. 3D). Increased levels of several cytokines were released in response to eHsp90α, although the magnitude to which eHsp90α stimulated cytokine release was notably lower than that stimulated by Aβ fibrils (Fig. 3D). In summary, we conclude that eHsp90α can stimulate microglia into an immune profile characterized by CXCL10 and CCL5 and an increase in the levels associated with NF-κB activation.

Extracellular Hsp90α mitigates fibrillary amyloid beta-induced neurotoxicity in vitro

We have previously reported a stalled inflammatory response in macrophages in the presence of eHsp90α (Murshid et al.

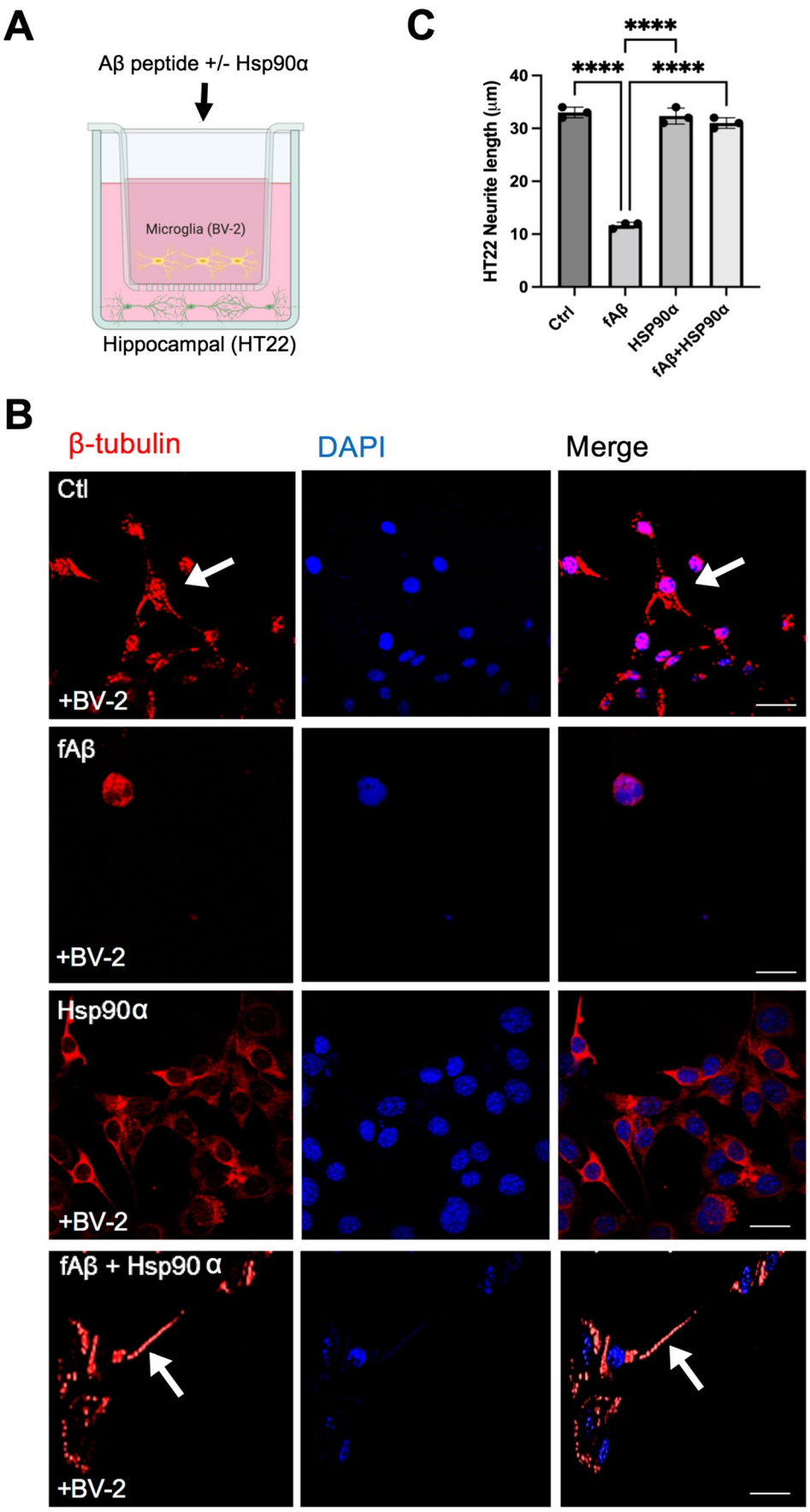

Fig. 4 Extracellular Hsp90α mitigates fibrillar Aβ-induced neurotoxicity in vitro. **A** Schematic for BV2 microglia and HT22 hippocampal neuron co-culture. **B** HT22 hippocampal neuronal cells were grown on coverslips in the bottom layer of a transwell culture dish. BV2 cells were then added to the top layer of the transwell and incubated with no ligand (Ctrl) fibrillar f-Aβ1-42 (2 μM) (fAβ), Hsp90α (10 μg/ml), or f-Aβ1-42 + Hsp90α as indicated for 72 h. After the 72-h incubation, HT22 cells from the bottom wells were then fixed with 4% para formaldehyde and then permeabilized with 0.1% Triton X-100 before staining with anti-β-tubulin antibodies. Stained cells on coverslips were then examined by confocal microscopy. Scale bar = 5 μm. **C** β-tubulin-stained neurite outgrowth was measured using ImageJ. A total of 100 cells were counted in each sample. ****$p < 0.0001$ and $n = 3$. Cartoon created with BioRender.com. Experiments were repeated three times with similar results

2015). As microglial inflammatory responses to Aβ fibrils are an important component of Aβ neurotoxicity, we next tested the hypothesis that eHsp90α protects against Aβ neurotoxicity associated with microglia-derived inflammation. To address this possibility, we co-treated murine microglial BV2 with purified Hsp90α and/or freshly prepared fibrillary Aβ1-42 (fAβ) and assessed the viability of adjacent neuronal HT22 cells potentially exposed to secreted microglial products via transwell culture preparations (Fig. 4A). BV2 cells pre-incubated with FITC fAβ-mediated toxicity towards the distant neuronal HT22 cells as indicated by extensive loss of microtubule-containing processes, a morphological measure of neuron cell viability (Hancock et al. 2015) (Fig. 4B). Within 72 h of fAβ incubation, many of the neuronal cells had lost their elongated processes (Fig. 4B). In contrast, when HT22 cells were co-cultured with BV2 cells that had been treated with both fAβ and eHsp90α in the top well of the transwell culture dish, the majority of the HT22 cells survived with neurite lengths comparable to those in the non-treated control, suggesting that addition of eHsp90α provided some protection against fAβ toxicity. eHsp90α treatment alone did not significantly impact neurite outgrowth (Fig. 4C). The extent of neurite outgrowth is quantified and is shown in Fig. 4C. Similar effects of exposure to fAβ with or without eHsp90α were also reported upon co-culture of HT22 neuronal cells with EOC2 microglial cells (A. Murshid, pre-print (Murshid et al. 2021)).

eHsp90α activates Nrf2 and promotes resistance to oxidative stress

In addition to gene ontology (GO) terms describing enrichment of processes related to inflammation and immunity, gene set enrichment GO analysis of the DEGs from EOC2 (Fig. 5A) and primary microglia (Suppl. Fig. 1A) treated with eHsp90α for 4 h or 12 h, respectively, also returned terms suggesting co-activation of an anti-oxidative stress response. When the genes contributing to these terms were examined (Fig. 5B; Suppl. Fig. 1B), many were also connected to the inflammatory signature described earlier; however, others such as upregulation of superoxide dismutase 2 *(Sod2)*, indicated a possible activation of the anti-oxidative stress response. When we considered this data with our recent finding that eHsp90α can stimulate indicators of Nrf2 activation (Murshid et al. 2021), we hypothesized that some level of Nrf2 co-activation may be occurring in response to eHsp90α and that this may provide a potential mechanism by which eHsp90α was able to mitigate fAβ toxicity. To investigate this prospect, we identified the top-10 differentially expressed Nrf2-target genes in terms of bidirectional fold change in each of the RNA-seq datasets (Fig. 5C). All the genes identified were found to be increased in eHsp90α-treated samples compared to untreated control samples, suggesting eHsp90α may stimulate Nrf2 transcriptional activity. To determine whether this response is common across microglial cells from different sources, we measured the levels of canonical Nrf2 target genes *Nqo1* and *Sod2* in BV2 cells treated with eHsp90α relative to untreated controls by RT-qPCR (Fig. 5D). To gain additional insight into the events associated with eHsp90α-stimulated Nrf2 activation, we assessed Nrf2 activating phosphorylation at Serine 40 by western blot (Fig. 5E). Nrf2 is phosphorylated at Ser40 under oxidative conditions by PKC kinases, a modification that mediates Nrf2 release from its negative regulator Keap1 (Numazawa et al. 2003; Huang et al. 2002), followed by its nuclear translocation and increased transcriptional activity. Treatment of EOC2 cells with eHsp90α led to increased levels of Nrf2 phosphorylation at S40 after both 4 and 24 h, accompanied by increased protein levels of p62, encoded by Nrf2 target *Sqstm1*, also observed at 24 h (Fig. 5E). To determine whether these indicators of Nrf2 activation were paired with attenuated production of oxidative molecules in response to inflammatory stimuli, we measured nitric oxide (NO) release from BV2 cells cultured with fAβ, eHsp90α, or co-treated with both fAβ and eHsp90α (Fig. 5F). Consistent with eHsp90α possessing Nrf2-activating properties, cells co-treated with both fAβ and eHsp90α exhibited reduced levels of NO production compared to the increased NO release by cells treated with fAβ alone (Fig. 5F). These findings indicate that in addition to moderate activation of microglial inflammatory responses, eHsp90α also induces Nrf2 a process that may limit microglial production of NO in response to fAβ.

eHsp90α stimulates expression of the scavenger receptor Marco in murine microglial cells

Microglia play important roles in Aβ metabolism and the inflammatory response to Aβ in Alzheimer's disease (Wilkinson and Khoury 2012). To gain some insight as to how eHsp90α may protect against the toxic effects of Aβ, we sought to identify eHsp90α — responsive mRNAs that may provide some basis for altered Aβ metabolism by BV2 microglial cells. We identified macrophage receptor with collagenous structure *(Marco)* as one such gene that was among the top-10 most differentially expressed genes in response to eHsp90α in the primary microglia RNA-seq dataset (Figs. 2C and 6A), and was also differentially expressed in the EOC2 dataset (Suppl. Fig. 2A). The encoded protein, Marco, is a scavenger receptor that has been identified as a microglial receptor for Aβ (Alarcon et al. 2005). Quantitation of *Marco* mRNA levels in eHsp90α-treated BV2 cells at 12 h found it to also be significantly upregulated compared to control untreated cells (Fig. 6B; Suppl. Fig. 2B), indicating *Marco* mRNA levels are induced by eHsp90α across multiple models of murine microglial cells. In eHsp90α treated BV2 cells, Marco protein levels were also observed to increase over a 24-h period in a concentration-dependent manner as

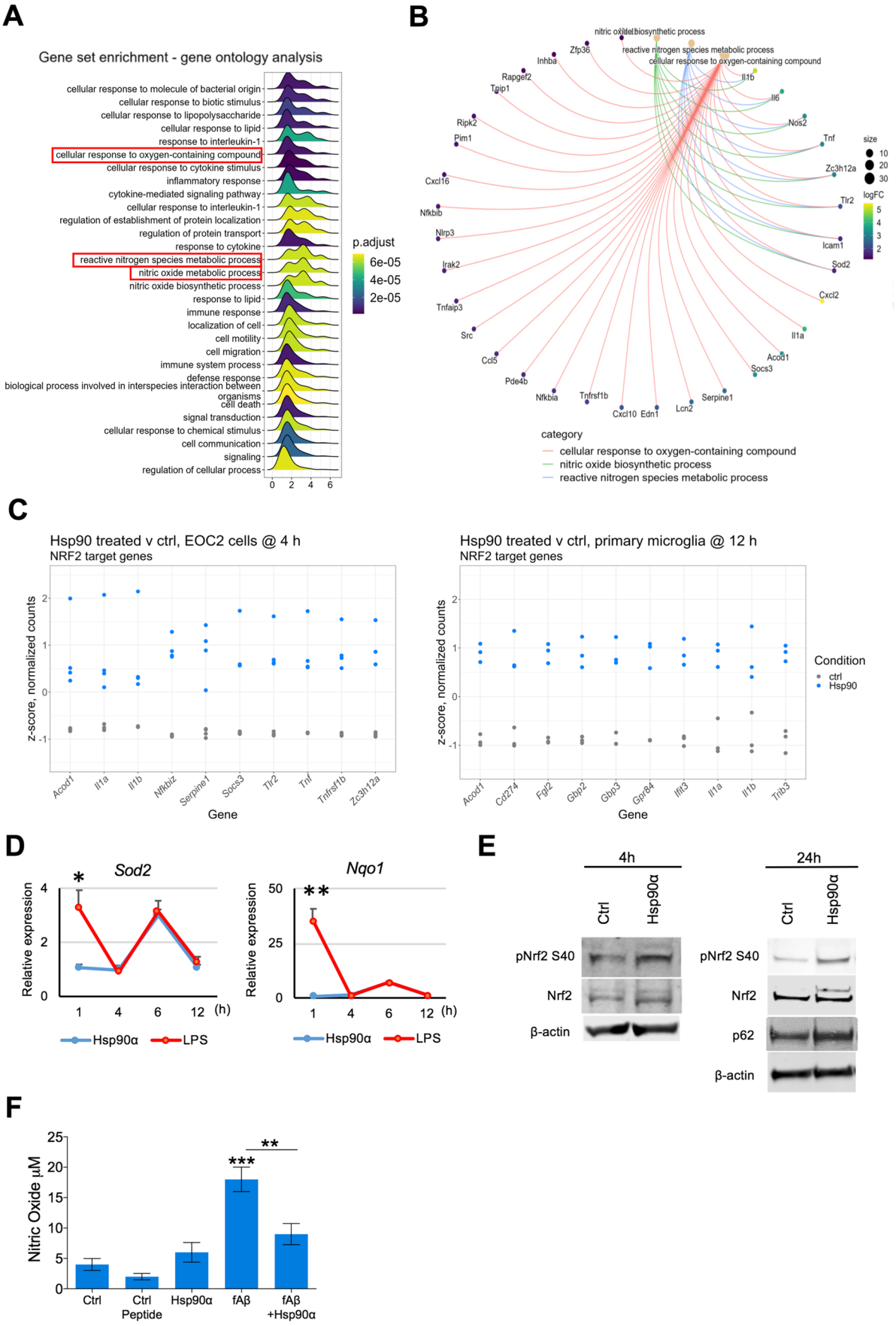
A
Gene set enrichment - gene ontology analysis
cellular response to molecule of bacterial origin
cellular response to biotic stimulus
cellular response to lipopolysaccharide
cellular response to lipid
response to interleukin-1
cellular response to oxygen-containing compound
cellular response to cytokine stimulus
inflammatory response
cytokine-mediated signaling pathway
cellular response to interleukin-1
regulation of establishment of protein localization
regulation of protein transport
response to cytokine
reactive nitrogen species metabolic process
nitric oxide metabolic process
nitric oxide biosynthetic process
response to lipid
immune response
localization of cell
cell motility
cell migration
immune system process
defense response
biological process involved in interspecies interaction between organisms
cell death
signal transduction
cellular response to chemical stimulus
cell communication
signaling
regulation of cellular process
p.adjust
6e-05
4e-05
2e-05
0 2 4 6
B
nitric oxide biosynthetic process
reactive nitrogen species metabolic process
cellular response to oxygen-containing compound
Zfp36
Inhba
Rapgef2
Tpip1
Il1b
Il6
Ripk2
Nos2
Pim1
Tnf
Zc3h12a
Cxcl16
Tlr2
Nfkbib
Nlrp3
Icam1
Irak2
Sod2
Cxcl2
Tnfaip3
Src
Il1a
Ccl5
Acod1
Socs3
Pde4b
Nfkbia
Tnfrsf1b
Cxcl10
Edn1
Lcn2
Serpine1
size
10
20
30
logFC
5
4
3
2
category
cellular response to oxygen-containing compound
nitric oxide biosynthetic process
reactive nitrogen species metabolic process
C
Hsp90 treated v ctrl, EOC2 cells @ 4 h
NRF2 target genes
z-score, normalized counts
Acod1
Il1a
Il1b
Nfkbiz
Serpine1
Socs3
Tlr2
Tnf
Tnfrsf1b
Zc3h12a
Gene
Hsp90 treated v ctrl, primary microglia @ 12 h
NRF2 target genes
z-score, normalized counts
Acod1
Cd274
Fgl2
Gbp2
Gbp3
Gpr84
Ifit3
Il1a
Il1b
Tnfb3
Gene
Condition
ctrl
Hsp90
D
Sod2
Nqo1
Relative expression
(h)
Hsp90α
LPS
E
4h
24h
Ctrl
Hsp90α
pNrf2 S40
Nrf2
β-actin
p62
F
Nitric Oxide μM
Ctrl
Ctrl Peptide
Hsp90α
fAβ
fAβ +Hsp90α

◂**Fig. 5** eHsp90α activates Nrf2 and promotes tolerance to oxidative stress. **A** Gene set enrichment GO analysis of DEG list of EOC2 cells treated with or without 10 µg/ml Hsp90α for 4 h. **B** ClusterProfiler cnetplot of DEG contributing to selected GO terms related to oxidative stress terms shown in (**A**). **C** Relative levels of mRNAs in EOC2 cells and primary microglia treated with or without 10 µg/ml Hsp90α for 4 h or 12 h, respectively, that were found to be differentially expressed and that have been identified as NRF2 regulatory targets within the curated datasets of the Chea3 TFEA software. The top 10 genes ranked by absolute logFC are shown. **D** BV2 cultured in 2% FBS media were treated with Hsp90α (10 µg/ml) or LPS (1000 ng/ml) for 1, 4, 6, and 12 h at which time RNA was isolated and quantified by qPCR for the indicated mRNAs. Gene expression is shown relative to *Actb* and normalized to untreated control RNA samples collected at the same time points. Control samples were treated with an equimolar concentration of His-tagged protein buffer sourced same vendor as the His-tagged Hsp90α. **E** Left: western blot analysis of pNrf2 S40, Nrf2 and β-actin in EOC2 cells 4 h after Hsp90α treatment. Right: western blot analysis of pNrf2 S40, Nrf2, p62, and β-actin levels in lysates of EOC2 cells at 24 h after Hsp90α treatment. **F** BV2 cells were incubated with the indicated ligands or with vehicle (ctrl) for 4–6 h. Control peptide was Aβ1-40. NO secretion to the medium was then quantitated using an Enzo nitric oxide quantitation assay kit, according to manufacturer's protocol

measured by Western blot (Fig. 6C). This was consistent with significantly higher levels of Marco immunostaining observed by confocal microscopy in BV2 cells after 24-h treatment (Fig. 6D) and a trend towards higher levels in eHsp90α treated EOC2 cells (Suppl. Fig. 2C). As previous studies have found *Marco* expression to be dependent upon Nrf2 (Reddy et al. 2009), we tested the hypothesis that the observed increase in *Marco* expression may be a product of eHsp90α-mediated Nrf2 activation. To address this possibility, we employed the chemical inhibitor of Nrf2, ML385, which decreases Nrf2 expression at the mRNA and protein levels over an extended treatment (Suppl. Fig. 2D). Consistent with a possible role for Nrf2 in eHsp90α-stimulated *Marco* expression, BV2 cells treated with both eHsp90α and ML385 exhibited significantly reduced *Marco* mRNA levels compared to samples treated with eHsp90α alone (Fig. 6E). Similarly, ML385 was also found to reduce eHsp90α-induced Marco protein levels as measured by quantification of the immunofluorescent staining by confocal microscopy (Fig. 6F). We therefore conclude that increased levels of eHsp90α stimulate expression of the Aβ-binding receptor Marco at both the mRNA and protein levels and that this effect may be a product of the observed eHsp90α-stimulated Nrf2 activation. Hsp90 also led to induction of Acod1 (cis-aconitate decarboxylase), known to induce TNFAIP3, also upregulated in both EOC2 and primary microglia RNA-seq datasets (Suppl. Tables 1, 2), which contribute to inflammatory modulation and the slight increase of NO upon Hsp90 stimulation alone (Wu et al. 2020). In addition, Clec4e (C-type lectin 4e) was one of the major upregulated genes (Fig. 1). Clec4e is a receptor for damage-associated molecular patterns (DAMPs) and necrotic cell bodies and may contribute to the complex phenotype initiated by eHsp90α (Clement et al. 2016).

Discussion

Our data suggest that exposure of microglia to eHsp90α leads to an altered phenotype that includes a mild activation of inflammatory genes in microglial cells. The effects observed included induction of cytokine genes and other genes associated with innate immunity and inflammation (Figs. 1, 2, 3) (Hanisch 2002; Lee et al. 2002). Microglia are thought to exist in a number of activation states, and these may involve both pro-and anti-inflammatory cytokine synthesis, depending on the stimuli (Janda et al. 2018). Our previous data indicated that microglial activation was associated with increased capacity to phagocytose amyloid-beta indicating that eHsp90 was able to concomitantly increase phagocytosis in combination with cytokine induction (Figs. 1, 2, 3; (Murshid et al. 2021)). Activation of microglia to an M1 type phenotype is associated with reduced phagocytosis in contrast to the effects of Hsp90 (Cherry et al. 2014). eHsp90α appeared to induce a complex gene expression phenotype, including stimulation of expression of both NF-kB and Nrf2 target genes. In RNA-seq analysis, Acod1 was upregulated by Hsp90 stimulation in both EOC2 and primary microglia (Fig. 5C). Acod1 induces TNFAP3 and suppresses NF-kB signaling (Wu et al. 2020). Indeed, the increases of NO and NF-kB expressions were slight with Hsp90 stimulation alone. Thus, there was a concomitant induction of pro-inflammatory genes dependent on NF-kB and anti-oxidant and anti-inflammatory genes in the antioxidant response (AOR) including Sod2 and Marco. The AOR protects cells against reactive oxygen species (ROS) through induction of a multi-gene expression cascade (Nguyen et al. 2003). Marco is an emerging anti-inflammatory receptor in mononuclear phagocytes that is induced by NRF2 (Fig. 6) and operating by directly represses Toll-like receptor 4 and stimulates the secretion of anti-inflammatory cytokine IL-37 (Fleur et al. 2021; Kissick et al. 2014). Nrf2 activation may provide protection from oxidative stress associated with innate activation of microglial cells (Branca et al. 2017).

Inflammation in the confined spaces of the CNS is a potential hazard and is generally kept under strict control (Hanisch 2002). eHsp90α appears to induce a desirable activation state in microglia, in which cytokines and phagocytosis are activated along with protective Nrf2 activation and anti-inflammatory gene expression (Figs. 1, 2, 3, 4). Indeed, exposure to the chaperone was able to protect neighboring neurons from the oxidative burst accompanying internalization of fAβ (Fig. 4). Beneficial effects appeared to include suppression of NO secretion by microglia treated with fAβ (Fig. 4). eHsp90 may thus play key homeostatic effects by accumulating in microglia and protecting from proteotoxic stresses and/or by inducing the AOR and reducing effects of ROS during the oxidative

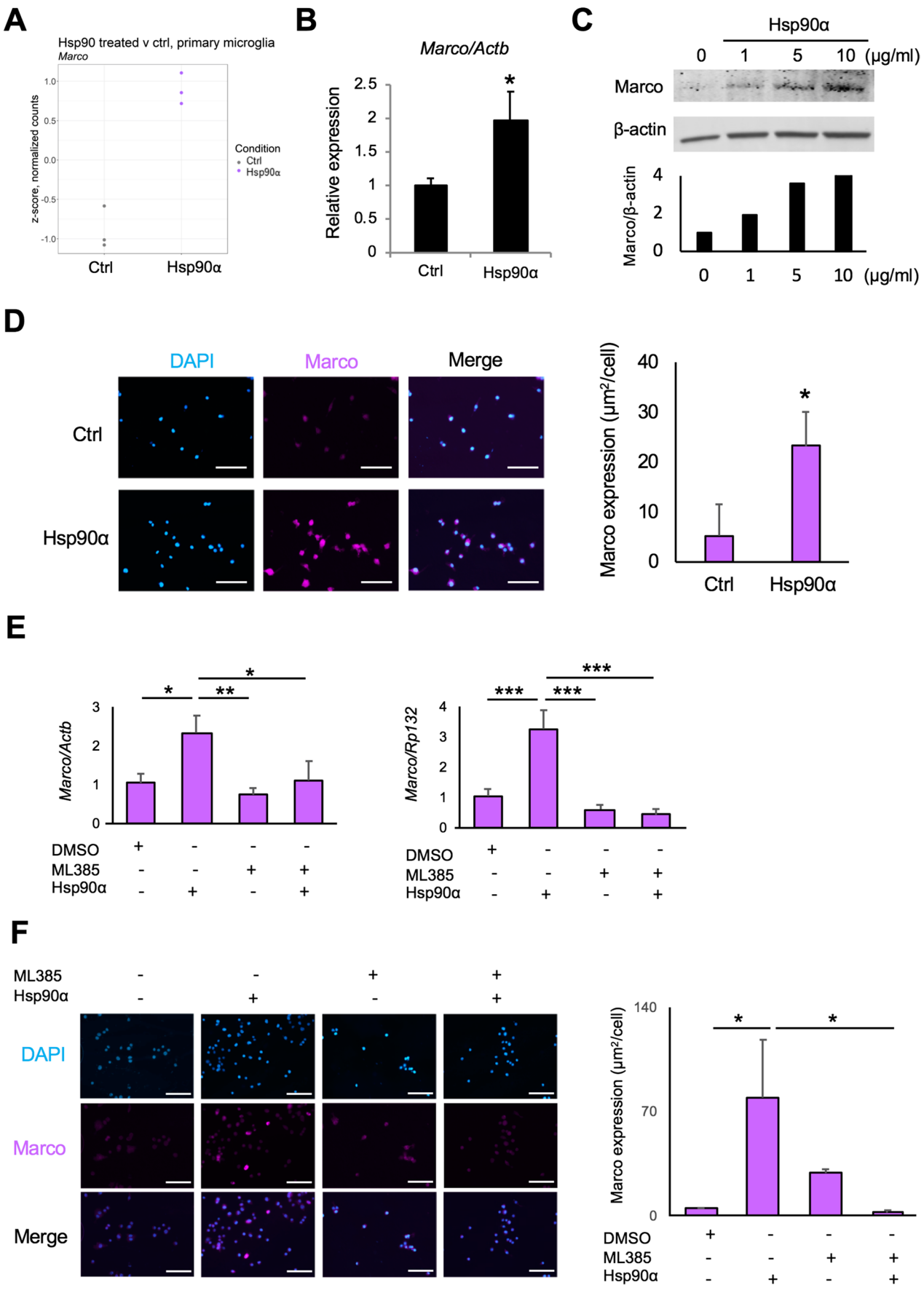
A
Hsp90 treated v ctrl, primary microglia
Marco
z-score, normalized counts
Condition
Ctrl
Hsp90α
B
Marco/Actb
Relative expression
C
Hsp90α
0 1 5 10 (μg/ml)
Marco
β-actin
Marco/β-actin
D
DAPI
Marco
Merge
Ctrl
Hsp90α
Marco expression (μm²/cell)
E
Marco/Actb
Marco/Rp132
DMSO
ML385
Hsp90α
F
ML385
Hsp90α
DAPI
Marco
Merge
Marco expression (μm²/cell)

◂**Fig. 6** eHsp90α stimulates expression of the scavenger receptor Marco in murine microglial cells. **A** Relative levels of *Marco* mRNA in primary microglia treated with or without 10 μg/ml Hsp90α for 12 h, quantified by RNA-seq. Relative levels shown are z-scores of TMM-normalized counts. Fold change was determined using the edgeR statistical package. **B** RT-qPCR quantitation of *Marco* normalized to *Actb* in BV2 cells after 12 h. $*p<0.05$, $n=4$. **C** Upper: western blot analysis of Marco and β-actin protein levels from BV2 cells treated Hsp90α for 24 h. Lower: quantitative analyses of Western blot for Marco. The relative values of Marco to β-actin are shown. **D** Left: immunocytochemistry staining of Marco (Magenta) in BV2 cells treated with 10 μg/ml Hsp90α for 24 h. Blue, DAPI. Scale bars, 100 μm. Right: analysis of Marco expression in BV2 cells treated with Hsp90α. $*p<0.05$, $n=3$. **E** RT-qPCR analysis of *Marco* mRNA in BV2 cells treated with 10 μg/ml Hsp90α and/or 5 μM ML385. The relative mRNA levels were normalized to *Actb* (left) or *Rpl32* (right), an internal control. $*p<0.05$, $**p<0.01$, $***p<0.001$, $n=3$. **F** Left: immunocytochemistry of Marco (Magenta) in BV2 cells treated Hsp90α and/or ML385. Blue, DAPI. Scale bars, 100 μm. Right: analysis of Marco expression in BV2 cells treated Hsp90α and/or 5 μM ML385. $*p<0.05$, $n=3$

burst accompanying phagocytosis. In addition, our previous studies showed that exposure to eHsp90 could direct internalized beta amyloid into the autophagy pathway which has been shown to reduce inflammatory effects (Murshid et al. 2021; Netea-Maier et al. 2016; Takahama et al. 2018).

Supplementary Information The online version contains supplementary material available at https://doi.org/10.1007/s12192-022-01279-9.

Acknowledgements We wish to thank the Department of Radiation Oncology for their continued support. Suraya Yasmine, Reeham Choudhury and Lay-Hong Ang are thanked for fine technical contributions. We thank Harvard Biopolymers Facility and Harvard Research Computing for their technical support. Figures 2A and 4A were made with Biorender.com.

Declarations

Conflict of interest The authors declare no competing interests.

References

Alarcon R et al (2005) Expression of scavenger receptors in glial cells. Comparing the adhesion of astrocytes and microglia from neonatal rats to surface-bound beta-amyloid. J Biol Chem 280(34):30406–15

Andrews S (n.d.) FastQC: a quality control tool for high throughput sequence data. Available online at: 2010; Available from: http://www.bioinformatics.babraham.ac.uk/projects/fastqc

Bolger AM, Lohse M, Usadel B (2014) Trimmomatic: a flexible trimmer for Illumina sequence data. Bioinformatics 30(15):2114–2120

Branca C et al (2017) Genetic reduction of Nrf2 exacerbates cognitive deficits in a mouse model of Alzheimer's disease. Hum Mol Genet 26(24):4823–4835

Calderwood SK, Gong J, Murshid A (2016) Extracellular HSPs: the complicated roles of extracellular HSPs in immunity. Front Immunol 7:159

Calderwood SK, Murshid A (2017) Molecular chaperone accumulation in cancer and decrease in Alzheimer's disease: the potential roles of HSF1. Front Neurosci 11:192

Cherry JD, Olschowka JA, O'Banion MK (2014) Neuroinflammation and M2 microglia: the good, the bad, and the inflamed. J Neuroinflammation 11:98

Clayton KA, Van Enoo AA, Ikezu T (2017) Alzheimer's disease: the role of microglia in brain homeostasis and proteopathy. Front Neurosci 11:680

Clement M et al (2016) Necrotic cell sensor Clec4e promotes a proatherogenic macrophage phenotype through activation of the unfolded protein response. Circulation 134(14):1039–1051

Dobin A et al (2013) STAR: ultrafast universal RNA-seq aligner. Bioinformatics 29(1):15–21

Frankish A et al (2019) GENCODE reference annotation for the human and mouse genomes. Nucleic Acids Res 47(D1):D766–D773

Fujimoto M et al (2005) Active HSF1 significantly suppresses polyglutamine aggregate formation in cellular and mouse models. J Biol Chem 280(41):34908–34916

Garigan D et al (2002) Genetic analysis of tissue aging in Caenorhabditis elegans: a role for heat-shock factor and bacterial proliferation. Genetics 161(3):1101–1112

Generation of anti-tumor immunity using mammalian heat shock protein 70 DNA (2006) 24(25)

Gong J et al (2018) Genotoxic stress induces Sca-1-expressing metastatic mammary cancer cells. Mol Oncol 12(8):1249–1263

Guzhova I et al (2001) In vitro studies show that Hsp70 can be released by glia and that exogenous Hsp70 can enhance neuronal stress tolerance. Brain Res 914(1–2):66–73

Hancock MK et al (2015) A facile method for simultaneously measuring neuronal cell viability and neurite outgrowth. Curr Chem Genom Transl Med 9:6–16

Hanisch UK (2002) Microglia as a source and target of cytokines. Glia 40(2):140–155

Heinz S et al (2010) Simple combinations of lineage-determining transcription factors prime cis-regulatory elements required for macrophage and B cell identities. Mol Cell 38(4):576–589

Hsu AL, Murphy CT, Kenyon C (2003) Regulation of aging and age-related disease by DAF-16 and heat-shock factor. Science 300(5622):1142–1145

Huang B et al (2010) Posttranslational modifications of NF-kappaB: another layer of regulation for NF-kappaB signaling pathway. Cell Signal 22(9):1282–1290

Huang HC, Nguyen T, Pickett CB (2002) Phosphorylation of Nrf2 at Ser-40 by protein kinase C regulates antioxidant response element-mediated transcription. J Biol Chem 277(45):42769–42774

Ikezu S et al (2020) Inhibition of colony stimulating factor 1 receptor corrects maternal inflammation-induced microglial and synaptic dysfunction and behavioral abnormalities. Mol Psychiatry

Janda E, Boi L, Carta AR (2018) Microglial phagocytosis and its regulation: a therapeutic target in Parkinson's disease? Front Mol Neurosci 11:144

Keenan AB et al (2019) ChEA3: transcription factor enrichment analysis by orthogonal omics integration. Nucleic Acids Res 47(W1):W212–W224

Kirkegaard T et al (2016) Heat shock protein-based therapy as a potential candidate for treating the sphingolipidoses. Sci Transl Med 8(355):355ra118

Kissick HT et al (2014) The scavenger receptor MARCO modulates TLR-induced responses in dendritic cells. PLoS One 9(8):e104148

Krasemann S et al (2017) The TREM2-APOE pathway drives the transcriptional phenotype of dysfunctional microglia in neurodegenerative diseases. Immunity 47(3):566-581. e9

La Fleur L et al (2021) Targeting MARCO and IL37R on immunosuppressive macrophages in lung cancer blocks regulatory T cells and supports cytotoxic lymphocyte function. Cancer Res 81(4):956–967

Lang BJ et al (2018) A workflow guide to RNA-seq analysis of chaperone function and beyond. Methods Mol Biol 1709:233–252

Lang BJ et al (2021) The functions and regulation of heat shock proteins; key orchestrators of proteostasis and the heat shock response. Arch Toxicol 95(6):1943–1970

Lee YB, Nagai A, Kim SU (2002) Cytokines, chemokines, and cytokine receptors in human microglia. J Neurosci Res 69(1):94–103

Li W, Sahu D, Tsen F (2012) Secreted heat shock protein-90 (Hsp90) in wound healing and cancer. Biochim Biophys Acta 1823(3):730–741

Murshid A et al (2015) Scavenger receptor SREC-I mediated entry of TLR4 into lipid microdomains and triggered inflammatory cytokine release in RAW 264.7 cells upon LPS activation. PLoS One 10(4):e0122529

Murshid A et al (2021) Extracellular Hsp90α Detoxifies β-amyloid fibrils through an NRF2 and autophagy dependent pathway. bioRxiv

Murshid A, Gong J, Calderwood SK (2010) Heat shock protein 90 mediates efficient antigen cross presentation through the scavenger receptor expressed by endothelial cells-I. J Immunol 185(5):2903–2917

Netea-Maier RT et al (2016) Modulation of inflammation by autophagy: consequences for human disease. Autophagy 12(2):245–260

Nguyen T, Sherratt PJ, Pickett CB (2003) Regulatory mechanisms controlling gene expression mediated by the antioxidant response element. Annu Rev Pharmacol Toxicol 43:233–260

Numazawa S et al (2003) Atypical protein kinase C mediates activation of NF-E2-related factor 2 in response to oxidative stress. Am J Physiol Cell Physiol 285(2):C334–C342

Okusha Y et al (2020) Rab11A functions as a negative regulator of osteoclastogenesis through dictating lysosome-induced proteolysis of c-fms and RANK surface receptors. Cells 9:2384

Rampelt H et al (2012) Metazoan Hsp70 machines use Hsp110 to power protein disaggregation. EMBO J 31(21):4221–4235

Reddy NM et al (2009) Innate immunity against bacterial infection following hyperoxia exposure is impaired in NRF2-deficient mice. J Immunol 183(7):4601–4608

Robinson MD, McCarthy DJ, Smyth GK (2010) edgeR: a bioconductor package for differential expression analysis of digital gene expression data. Bioinformatics 26(1):139–140

Stansley B, Post J, Hensley K (2012) A comparative review of cell culture systems for the study of microglial biology in Alzheimer's disease. J Neuroinflammation 9:115

Takahama M, Akira S, Saitoh T (2018) Autophagy limits activation of the inflammasomes. Immunol Rev 281(1):62–73

Taylor AR et al (2007) Regulation of heat shock protein 70 release in astrocytes: role of signaling kinases. Dev Neurobiol 67(13):1815–1829

Thawkar BS, Kaur G (2019) Inhibitors of NF-kappaB and P2X7/NLRP3/caspase 1 pathway in microglia: novel therapeutic opportunities in neuroinflammation induced early-stage Alzheimer's disease. J Neuroimmunol 326:62–74

Theriault JR, Adachi H, Calderwood SK (2006) Role of scavenger receptors in the binding and internalization of heat shock protein 70. J Immunol 177(12):8604–8611

Tidwell JL, Houenou LJ, Tytell M (2004) Administration of Hsp70 in vivo inhibits motor and sensory neuron degeneration. Cell Stress Chaperones 9(1):88–98

Timmerman R, Burm SM, Bajramovic JJ (2018) An overview of in vitro methods to study microglia. Front Cell Neurosci 12:242

van Oosten-Hawle P, Morimoto RI (2014) Transcellular chaperone signaling: an organismal strategy for integrated cell stress responses. J Exp Biol 217(Pt 1):129–136

Wang X, Seed B (2003) A PCR primer bank for quantitative gene expression analysis. Nucleic Acids Res 31(24):e154

Wilkinson K, El Khoury J (2012) Microglial scavenger receptors and their roles in the pathogenesis of Alzheimer's disease. Int J Alzheimers Dis 2012:489456

Wu R et al (2020) ACOD1 in immunometabolism and disease. Cell Mol Immunol 17(8):822–833

Yamamoto M et al (2008) Cytokine-mediated inhibition of fibrillar amyloid-beta peptide degradation by human mononuclear phagocytes. J Immunol 181(6):3877–3886

Yu G et al (2012) clusterProfiler: an R package for comparing biological themes among gene clusters. OMICS 16(5):284–287

Zhang Y et al (2018) TREM2 modulates microglia phenotypes in the neuroinflammation of Parkinson's disease. Biochem Biophys Res Commun 499(4):797–802